RESEARCH ARTICLE

NANO · MICRO small
www.small-journal.com

[n]Cycloparaphenylenes as Compatible Fluorophores for Melt Electrowriting

Patrick C. Hall, Harrison W. Reid, Ievgenii Liashenko, Biranche Tandon, Kelly L. O'Neill, Naomi C. Paxton, Gabriella C. J. Lindberg, Ramesh Jasti, and Paul D. Dalton**

Fluorescent probes are an indispensable tool in the realm of bioimaging technologies, providing valuable insights into the assessment of biomaterial integrity and structural properties. However, incorporating fluorophores into scaffolds made from melt electrowriting (MEW) poses a challenge due to the sustained, elevated temperatures that this processing technique requires. In this context, [n]cycloparaphenylenes ([n]CPPs) serve as excellent fluorophores for MEW processing with the additional benefit of customizable emissions profiles with the same excitation wavelength. Three fluorescent blends are used with distinct [n]CPPs with emission wavelengths of either 466, 494, or 533 nm, identifying 0.01 wt% as the preferred concentration. It is discovered that [n]CPPs disperse well within poly(ϵ-caprolactone) (PCL) and maintain their fluorescence even after a week of continuous heating at 80 °C. The [n]CPP-PCL blends show no cytotoxicity and support counterstaining with commonly used DAPI (Ex/Em: 359 nm/457 nm), rhodamine- (Ex/Em: 542/565 nm), and fluorescein-tagged (Ex/Em: 490/515 nm) phalloidin stains. Using different color [n]CPP-PCL blends, different MEW fibers are sequentially deposited into a semi-woven scaffold and onto a solution electrospun membrane composed of [8]CPP-PCL as a contrasting substrate for the [10]CPP-PCL MEW fibers. In general, [n]CPPs are potent fluorophores for MEW, providing new imaging options for this technology.

1. Introduction

Electrohydrodynamic (EHD) processing includes multiple manufacturing technologies, including solution electrospinning (SES),[1–3] melt electrospinning,[4] electrospraying,[3] and melt electrowriting (MEW).[5] Products of these technologies have been investigated for textile,[6,7] filtration[8,9] and tissue engineering (TE) applications.[10,11] SES, in particular, has been widely investigated over the past two decades.[2,12] As a nozzle-based fabrication technology, its simplicity helped spark its adoption for research, with small-diameter (typically <1 μm) SES fibers that were especially investigated for biomedical applications.[2,13]

SES primarily produces non-woven membranes from sub-micron diameter fibers using an EHD phenomenon of jet instability, often referred to as "whipping".[14,15] After an applied voltage generates surface charges that overcome the drop surface tension, a jet (i.e., a fluid column) is ejected that is initially straight. As the surface charges on the jet surface increase in density along its length toward the collector,[15] they further stretch and spiral the jet to form small diameter fibers. SES membranes are non-woven as jet whipping makes it difficult to place fibers in a specific location.

A different, but configurationally similar technology is melt electrowriting (MEW), that produces well-positioned fibers but leverages a different EHD effect.[16,17] When applying a high voltage to a fluid column (i.e., a jet), the charges generated can prevent Plateau–Rayleigh instabilities,[17,18] allowing the flow rate to the fluid column to be substantially reduced.[16] With a thin, stable electrified jet achieved, the nozzle is moved relative to collector to deposit small diameter fibers (typically between 1 and 50 μm) with high accuracy.[19,20] Using additive manufacturing principles, this microfiber from the molten jet is repeatedly stacked upon each other. MEW scaffolds are tunable with a porosity ranging from 80–98%[21] that are easily populated with cells/tissues.[22–24]

Since this technique is primarily used for biomedical applications, including include single fiber studies, the visualization of the individual MEW fibers is an important property to attain. This aspect complements the many applications of MEW scaffolds,

P. C. Hall, I. Liashenko, B. Tandon, K. L. O'Neill, N. C. Paxton, G. C. J. Lindberg, R. Jasti, P. D. Dalton
Phil and Penny Knight Campus for Accelerating Scientific Impact
University of Oregon
1505 Franklin Boulevard, Eugene, OR 97403-6231, USA
E-mail: rjasti@uoregon.edu; pdalton@uoregon.edu
H. W. Reid, R. Jasti
Department of Chemistry and Biochemistry & Materials Science Institute
University of Oregon
1505 Franklin Boulevard, Eugene, OR 97403-6231, USA
B. Tandon
Microsystems Laboratory
École Polytechnique Fédérale de Lausanne (EPFL)
Lausanne CH-1015, Switzerland
N. C. Paxton
Centre for Biomedical Technologies (CBT)
Queensland University of Technology (QUT)
2 George St, Brisbane, QLD 4000, Australia

The ORCID identification number(s) for the author(s) of this article can be found under https://doi.org/10.1002/smll.202400882

DOI: 10.1002/smll.202400882

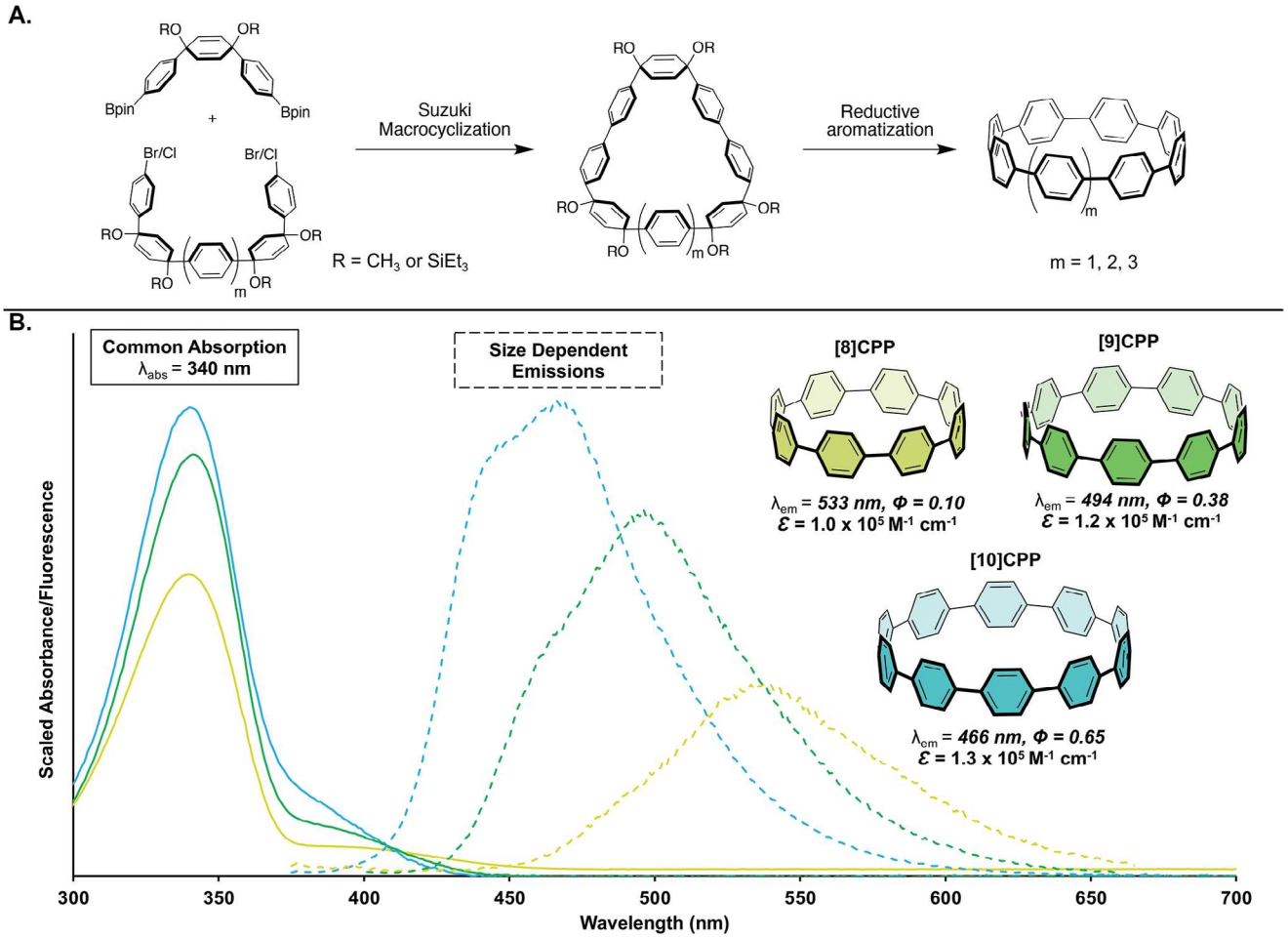

Figure 1. A) General synthetic scheme for [n]CPPs sized n = 8, 9, 10. B) Optoelectronic properties of [n]CPPs with absorbance (solid) and emission (dashed) spectra shown along with corresponding excitation maxima (λ_{abs}), emission maxima (λ_{em}), quantum yield (Φ), and molar extinction coefficient (ϵ) for each of the [n]CPPs examined in this work.

which include blood vessel engineering,[25] heart valves[26] and patches,[27] skin grafts,[28] including in vivo use where the exact locations of different fibers aid in the understanding the biomaterials science. Examples for MEW scaffolds include higher harmonic multiphoton microscopy for intravital imaging,[29] confocal microscopy of 3D in vitro constructs,[30] and histology after in vitro culture[11] or implantation.[31] Due to their small fiber diameters, MEW scaffolds are challenging to discern without using a fluorescent probe. Fluorophores embedded within the melt, however, must withstand elevated temperatures for sustained periods so that they can be processed. A recent study by Wu et al. introduced fluorescence to MEW scaffolds through the incorporation of fluorescent nanodiamonds that provide a single emission band.[32] Another study used a biomaterial ink specifically designed for MEW hydrogels that chemically binds the fluorophore when placed into a rhodamine solution[33] in a second step.

In this work, we investigate fluorescence in MEW scaffolds from PCL by using [n]cycloparaphenylenes ([n]CPPs) as a blended additive with tailorable fluorescent properties. They have thermal stability and have been shown to be cytocompatible when conjugated to an antibody.[34] [n]CPPs, commonly referred to as "nanohoops", are a type of carbon nanomaterial described as the shortest cross-section of an armchair carbon nanotube. First synthesized in 2008 by Jasti and Bertozzi, [n]CPPs are unique from other nanocarbons in their ability to be precisely synthesized via bottom-up methodologies with common synthetic starting materials and reagents (**Figure 1A**). This building-block approach has led to the synthesis of a number of different-sized [n]CPPs from [5]CPP-[18]CPP (where "n" is the number of phenylene rings) along with numerous functionalized derivatives. The centrosymmetric nature of the nanohoops coupled with their strained radially oriented pi-conjugated systems also enables several intriguing optoelectronic properties. First, unlike linear pi-conjugated molecules, these strained macrocycles have shrinking HOMO-LUMO gaps with decreasing ring size. Consistent with this trend, the [n]CPPs have a redshifting emission as the CPP ring size decreases. However, [n]CPPs possess a common absorption at 340 nm regardless of ring size or number of rings. This unique feature is ideal for multiplexing applications where only one excitation source is required.[35] Moreover, it is noteworthy that these nanohoops have molar absorption coefficients on the order of

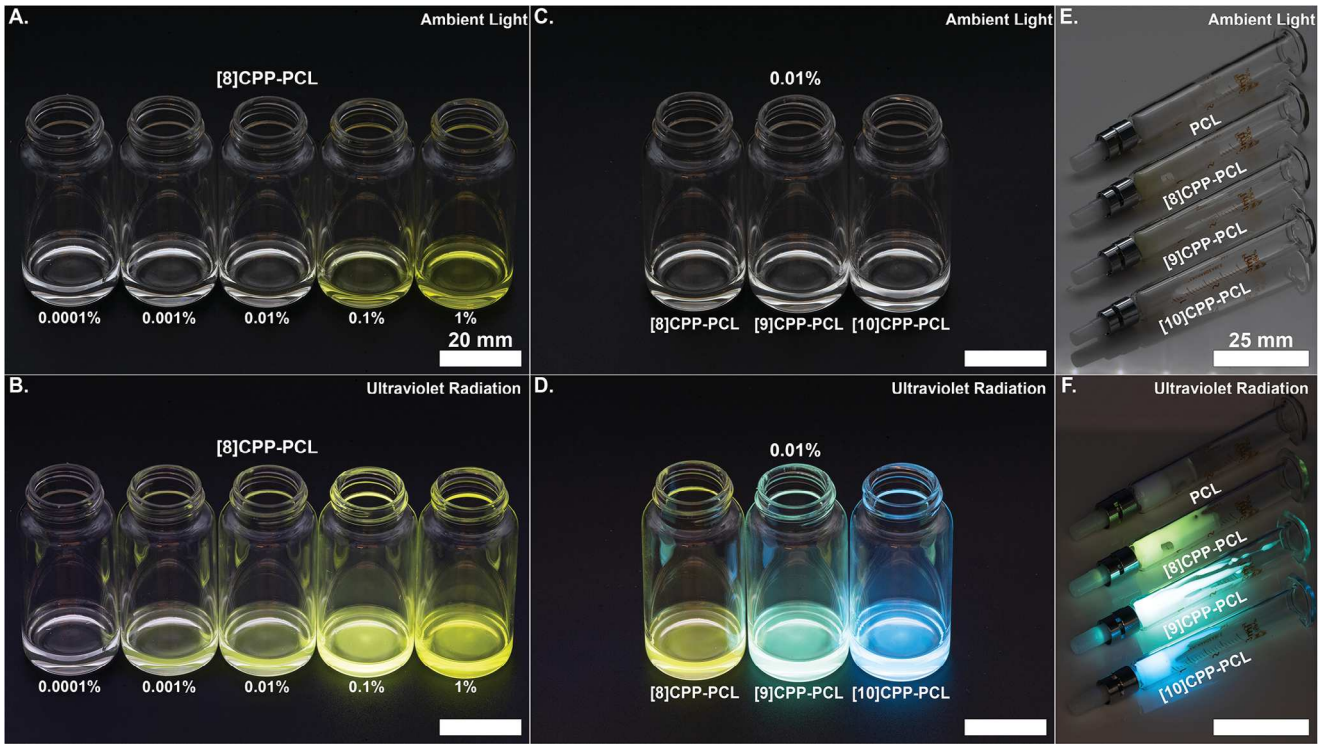

Figure 2. General fluorescence of [n]CPP blends with PCL. Different concentrations of [8]CPP dissolved in a 20 wt% PCL-DCM solution shown under A): Ambient light and B): UV radiation excitation with concentrations arranged logarithmically from 0.0001% by weight to 1% by weight, left to right. C,D): 0.01% [8], [9], and [10]CPP-PCL dissolved in DCM under visible and UV radiation. Solvent-removed PCL blended with 0.01% [8], [9], and [10]CPP-PCL in glass syringes under E) visible and F) illuminated with UV radiation.

10^5 M^{-1} cm^{-1}, which coupled with the high quantum yield leads to exceptionally bright fluorescent material.

Interestingly, only one study has utilized the optoelectronic properties of [n]CPPs as an additive in a polymeric material.[36] It was reported that the addition of [6]CPP up to 5 wt% improved the stretchability of a diketopyrrolopyrrole-based semiconducting polymer while maintaining its mobility. However, to our knowledge, no study has probed the possibility of [n]CPPs serving as fluorescent-capable additives despite offering several materials advantages. Specifically, [n]CPPs are soluble in common organic solvents (e.g., DCM, THF) that makes them compatible for mixing with many polymers used with EHD technologies. Additionally, [n]CPPs are thermally stable with a thermal degradation temperature above 300 °C for n > 7; exceeding the temperatures requirements for MEW of PCL and other polymers.[37,38]

2. Results and Discussion

The blending of [n]CPPs with PCL yielded excellent fluorescent properties after exposing them to UV radiation (**Figure 2**). A range of concentrations was visualized under both ambient light and UV radiation excitation conditions, with [8]CPP concentrations from 0.0001 wt% up to 1 wt% (Figure 2A,B). The optimal ratio of [8]CPP to PCL was determined to be 0.01 wt%, since it provided the bulk material with a strong fluorescent signal (Figure 2B,D), but without fluorescence or color bias occurring under ambient light (Figure 2A,C).

This lack of fluorescence to the naked eye under ambient light was also observed at 0.01 wt% for both [9]CPP-PCL and [10]CPP-PCL samples (Figure 2C). The fluorescent capabilities of [n]CPPs and [n]CPP-PCL blends provide additional dimensions for microscopy, as the multiple emission wavelengths result from the singular excitation wavelength. While the [n]CPPs have an absorption peak at 340 nm, readily available UV flashlights that use 365 nm still result in bright emissions, even at such low concentrations, with a redshift occurring as the [n]CPP's cyclic radius decreases. This redshift results in the [8], [9], and [10]CPP having fluorescent emissions in the 533, 494, and 466 nm wavelengths respectively. The reason for this common absorbance is due to the CPPs having Laporte-forbidden HOMO-LUMO transitions coupled with the fact that the higher energy-allowed transitions (e.g., HOMO to LUMO+1) are similar in energy for all nanohoop sizes.[38] In contrast, the emissive properties of [n]CPPs arise from exciton localization in the excited state that causes a breaking of the centrosymmetry of the nanohoop, and therefore becomes an allowed emission.[39]

2.1. Influence of CPP on Composite Thermal and Viscoelastic Properties

The thermal analysis of the PCL and [n]CPP-PCL blends was performed to assess the impact of CPP inclusion on the physical properties of the material influencing printability and mechanical properties compared to PCL alone (**Figure 3**). PCL used in

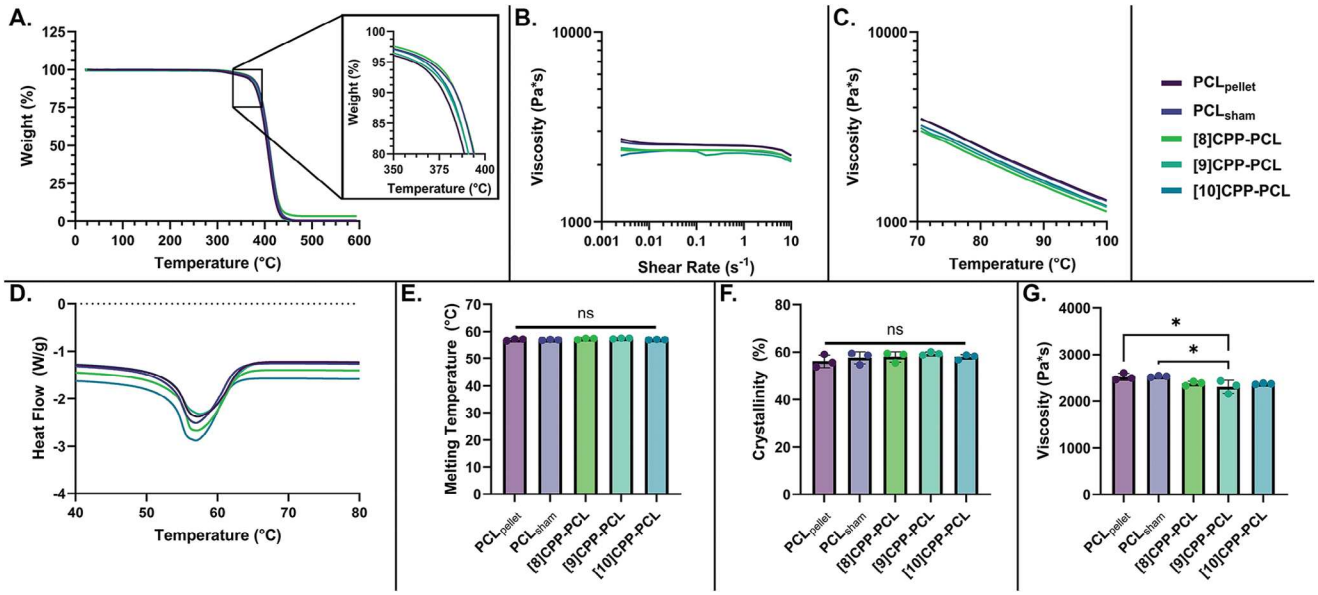

Figure 3. Thermal and viscoelastic properties of [n]CPP-PCL. A) Thermogravimetric analysis of [n]CPP-PCL compared to PCL_{pellet} and PCL_{sham}. B) Viscosity analysis of [n]CPP-PCL materials as related to shear rate at 80 °C. C) Viscosity analysis of [n]CPP-PCL materials as related to temperature at 1 Hz. D) Differential scanning calorimetry of [n]CPP-PCL materials. E) Melting temperature of all materials. F) Percent crystallinity of all materials. G) Viscosity of all materials at 1 Hz and 80 °C.

its original pellet form is termed PCL_{pellet} and a PCL control that was solvent mixed (but no fluorophore added) is termed PCL_{sham}. DSC analysis revealed no significant difference in the melting temperature (average of 57.1 ± 0.3 °C) and no significant difference in the crystallinity (average of 57.8 ± 2.0%) (Figure 3D–F). At a concentration of 0.01 wt%, the melting properties of the composite were dominated by the PCL phase, and importantly, the processing steps by which the CPP was incorporated into the PCL did not impact the thermal properties of the material. No significant difference was found between the melting temperature and crystallinity of virgin, unprocessed PCL (PCL_{pellet}) compared to a PCL sample that had undergone the same blending conditions without the addition of the fluorophores (PCL_{sham}) (Figure 3E,F).

Similarly, degradation measurements further validated the assertion that no significant difference in material thermal properties was observed as a result of the inclusion of CPP and processing steps (Figure 3A). All curves show highly repeatable degradation behavior, with negligible differences in degradation onset observed after ≈300 °C (Figure 3A, inset). The use of vacuum and heat evaporation was validated in successfully removing DCM from the samples, whereby no mass loss was observed around the boiling point of DCM at 39.6 °C ($n = 3$, $p = 0.001$), with all CPP samples measuring 99.993 ± 0.003% of initial mass (Figure 3D).

Rheology measurements further validated the limited impact of CPP inclusion on the viscoelastic properties of the samples (Figure 3B,C). Near-Newtonian behavior was observed in all samples, with some mild shear thinning observable approaching 10 s^{-1} (Figure 3B). These results are consistent with the typical behavior of PC12 reported previously[40,41] and indicate that the addition of the CPP and processing steps posed no substantial difference to the materials' viscosity over the shear range examined. For example, a marginal difference in viscosity was observed at 1 s^{-1} between the CPP-inclusive, with viscosity of 2345 ± 82 Pa s, compared to PCL-only samples, with viscosity of 2524 ± 48 Pa s ($n = 3$, $p = 0.01$), indicating that the CPP slightly reduced the viscosity of the material at this shear rate (Figure 3G). Similarly, in characterizing the thermoresponsive properties of the materials, the sub order-of-magnitude decrease in viscosity is characteristic of PCL samples previously studied and no substantial difference in thermoresponsivity was observed with the inclusion of CPP. The marginal difference in viscosity over the shear rates tested did not significantly impact printability, and as such, the CPP composites could be fabricated with the same MEW operational parameters as PCL_{pellet}.

Overall, the inclusion of CPP within the PCL instigated a negligible difference in thermal and viscoelastic properties compared to PCL alone, whereby no meaningful difference in the melting temperature, crystallinity, degradation profile, or bulk viscoelastic properties was observed. This validation data critically underpins the utility and translatability of this new MEW material. The extensive research and established knowledge base surrounding PCL can be directly applied to this new composite, circumventing the need for additional foundational studies using this new material.

2.2. MEW of [n]CPP-PCL Blends

As can be seen in Figures 2E,F, the fluorescent properties of the [n]CPP and PCL blend "inks" after solvent removal are well maintained. For high-resolution additive manufacturing of the materials, MEW was chosen for its reproducibility and stability compared to other direct electrohydrodynamic writing techniques that involve solvent dissolution of polymers. MEW, however, imparts challenging thermal conditions on the polymer to be processed, due to the nature of the technology.[42] The mechanism

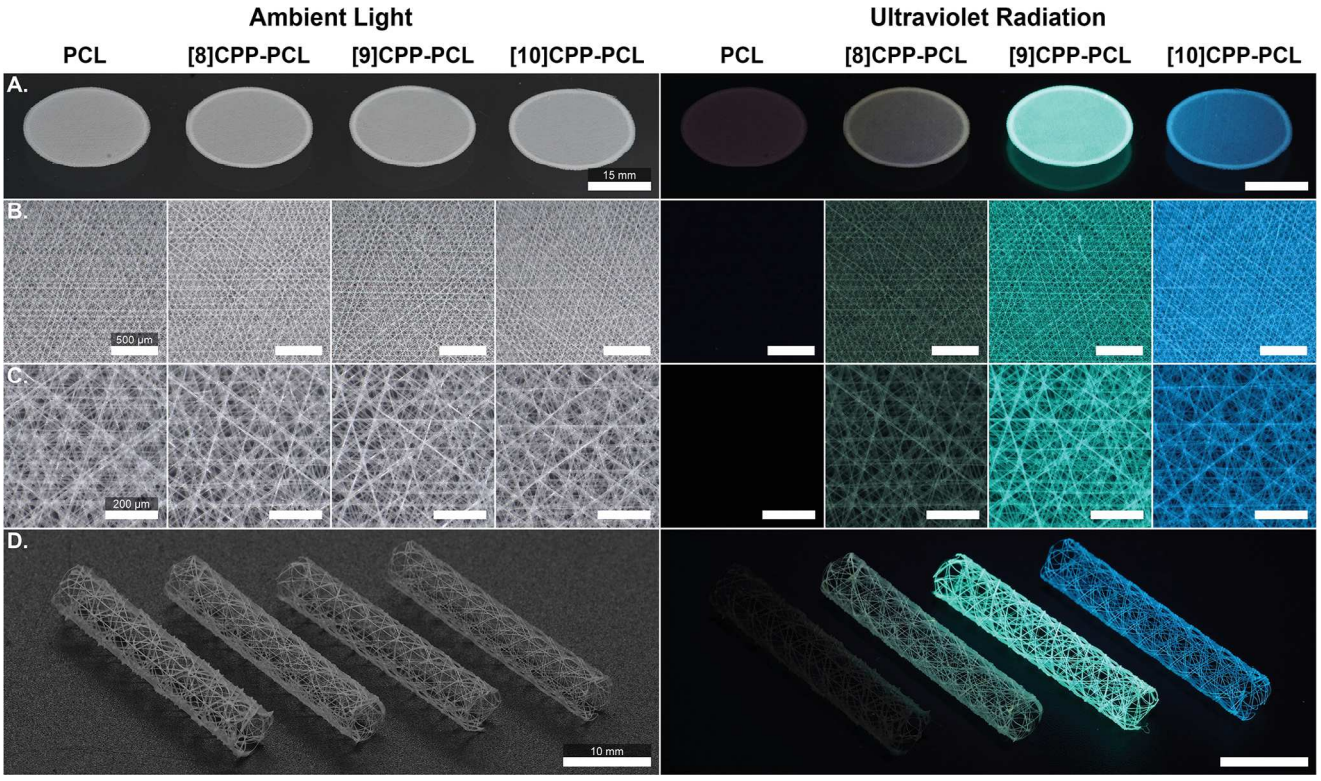

Figure 4. MEW of [n]CPP-PCL: Entire scaffold images under A–C) ambient and UV radiation. B) Low magnification of scaffolds shows how fluorescent capabilities are retained on a fiber-specific basis. C) High magnification of scaffolds shows the capabilities of [n]CPP-PCL in imaging fine scale properties with bulk fluorescent distribution. D) Tubular MEW scaffolds retain fluorescence after printing.

to achieve small diameters for MEW is via extremely low flow rates to the nozzle, down to 2–5 µL h^{-1}.[42,43] This low throughput results in the polymer in the syringe remaining heated for substantial periods of time. Preferably [n]CPP-PCL blends must be thermally resistant for at least a week in such processing conditions, as there is convenience in not constantly replacing the syringe with fresh material. When printing with PCL, it is typically heated to 75–85 °C. Therefore, any fluorophores to be included with the PCL must be thermally resistant at 85 °C for periods up to 1 week without significant loss in their fluorescent capabilities for a comparable duration. **Figure 4** shows that indeed the fluorescent capabilities of [n]CPPs are retained after the challenging MEW processing conditions. While scaffolds retain a white appearance under ambient light (Figure 4A,D), under UV illumination they provide emissions in the corresponding wavelengths for the [n]CPPs. Furthermore, from our experience working with the [n]CPP/PCL blend, multi-week-long heating of the syringe at 80 °C did not noticeably affect the prints or their robust fluorescence.

The MEW processability was determined through measuring the jet speed, the collector speed at which the deposited fiber transitions from buckled to straight. This measurement can determine whether the inclusion of the [n]CPPs affects this important processing parameter. The addition of the [n]CPP's to PCL followed by extensive solvent removal steps was shown to not affect the jet speed at the same printing parameters. We did not see statistically significant differences between the fiber diameters, which is shown in Figure S1 (Supporting Information), with an average fiber diameter across all samples of 10.04 ± 0.569 µm.

A scaffold design was composed of 40 layers of straight fibers spaced at 150 µm, where each next layer was rotated by 36° (180°/5 directions), printed with processed PCL and [8], [9], and [10]CPP-PCL then imaged on various scales under ambient and UV radiation. Figure 4 provides the overview that visualizes the fluorescent capability of [n]CPP-PCL, ranging from the centimeter down to micrometer scale imaged with a digital camera then optical microscope. Furthermore, several tubular MEW scaffolds were designed with different morphologies, including a 30° angular displacement between each layer to generate structures not typical for a classically wound tube (Figure 4D).

2.3. Cytotoxicity of [n]CPP-PCL Blends

Since the [n]CPPs will be incorporated within MEW fibers as part of scaffolds for biomedical applications, their cytotoxicity must be determined. Previous investigations that used functionalized [n]CPPs for in vivo cell imaging showed no appreciable cytotoxicity, but it remains unknown how the blended nanohoops would behave in this environment.[34,44] **Figure 5** confirmed that the different [n]CPP-PCLs do not demonstrate in vitro cytotoxicity in accordance with ISO 10993-5 and ISO 10993-12 methods.

As shown in Figure 5, all [n]CPP-PCL scaffold elutions displayed cytocompatible responses in the presence of

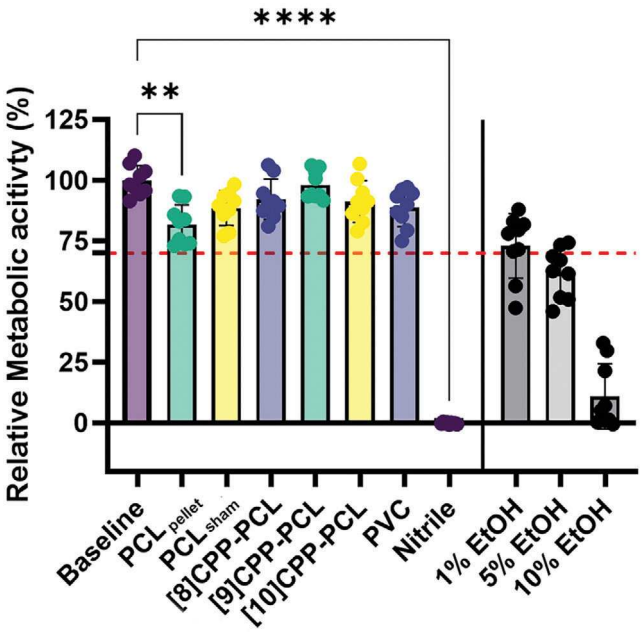

Figure 5. In vitro analysis of [n]CPP-PCL Cytotoxicity of [n]CPP-PCL compared to PCL control. ** = $p < 0.005$; **** = $p < 0.0001$; $n = 9$.

mesenchymal stem cells (MSC), with relative metabolic activity recorded above the 70% threshold for all samples. MSCs were chosen for their applicability to biofabrication, as well as their sensitivity compared to other common cell types used in cytotoxicity testing, like fibroblasts. It was furthermore observed that all the [n]CPP-PCL blends yielded cell proliferation responses comparable to PCL_{sham}. Further validation of the applied scaffold extract testing protocol was achieved through the inclusion of positive (PVC) and negative (Nitrile) material controls. Additionally, the sensitivity of the assay was confirmed by exposing it to an ethanol concentration gradient. This gradient demonstrated that concentrations of both 5% and 10% ethanol resulted in a cytotoxic read-out (<70% relative metabolic activity), while 1% ethanol is not enough to yield toxic effects in vitro. Further view of the other controls used in this study are seen in Figure S3 (Supporting Information). Overall, >90% relative metabolic activity was recorded on average across all [n]CPP-PCL variants, which indicates that this material is suitable as an in vitro or in vivo scaffold tag and imaging guide.

A potentially confounding factor in the imaging and cytotoxicity of the [n]CPP-laden fibers is whether the fluorophore leaches out of the [n]CPP-PCL with time. Leaching tests conducted on slabs of material proved the stability of the blending of the fluorophores in PCL, as shown in Figure S2, (Supporting Information) with the ultraviolet spectroscopy of the leached PBS proving a minimal leaching. Compared with the processing controls, it is shown that no measurable amount of the [n]CPPs leach from the polymer into PBS. However, some residual DCM from the mixing process is seen leaching into the PBS solution, as indicated by a peak at 203 nm. In accordance with the results stated above, the residual amounts of DCM found in PBS did not inhibit cell metabolic activity.

2.4. Fluorescent Staining of Seeded Cells on [n]CPP-PCL Scaffolds

To investigate the usability of the CPP-PCL materials within a bioengineering context, seeding of MSCs onto CPP-PCL MEW scaffolds showed the relation of fluorescence between the materials and common fluorophores. The seeding was conducted onto scaffolds with the intention of investigating whether commonly applied DAPI, rhodamine and fluorescein stains would be visible against the CPP-PCL materials. (Figure S4A, Supporting Information) Cells were seeded onto the scaffolds by first suspending them at a concentration of 5m cells/mL, then pipetting 12 µL of cell suspension onto dry scaffolds. Every 2nd hour, 5 µL of media was added to the scaffolds, until hour 6, wherein the scaffolds were immersed in excess media. No secondary structures were used to hold the scaffolds in place, and the seeding processes ensured that the scaffolds did not retain surface tension and float on top of the media. After approaching confluency at 6 days of culture, the scaffolds were fixed then stained. As shown in **Figure 6**, human adipose stem cells attach to all MEW scaffold formulations and demonstrate typical growth behavior to that of a square-shaped porous scaffold. Specifically, cells adhere along the fibers and triggers the deposition of cytoskeleton, resulting in rounded corners and the formation of a distinct central opening.

Results furthermore revealed that the fluorescent materials are visible together with traditional fluorescent DNA and filamentous actin probes using cytochemical cytochemical techniques. Through the use of preexisting filter and laser assemblies, all [n]CPP-PCL materials were easily visible against the common stains. The contrast of [8]CPP-PCL and [9]CPP-PCL from DAPI, rhodamine, and fluorescein is notable, as the emission and excitation spectra of these materials has minimal overlap with these common fluorophores. However, [9]CPP-PCL has strong specificity in its individual channel, but still is visible in the DAPI channel. Overall, the fluorescence of these materials does not overpower the DAPI signal and can facilitate analysis of cell-scaffold interactions. The strong fluorescent signal of all materials across common emission wavelengths, while still remaining specific to the scaffolds indicates high usability as in vitro and in vivo imaging tags. Overall, the investigated [n]CPP-PCL blends showcase fluorescent properties that can be customized to various imaging needs of biological samples.

2.5. SES of [n]CPP-PCL

Several groups have recently performed MEW onto SES membranes to form skin,[11] blood vessels[45] in vitro and wound dressings.[46] As an example, we imparted fluorescence into SES membranes using CPPs (**Figure 7**A,B) and performed MEW onto this substrate with [n]CPP-PCL blend. With the [n]CPPs dissolved into a PCL polymer solution, the electrospinning of fibers was performed using a standard SES apparatus and as expected, the resulting non-woven membranes fluoresced. This is a simple approach for SES, as solvent dissolution is already part of the workflow.

Further visualization of SES membranes using SEM showed that there was only a slight variation of fiber diameters for the different [n]CPPs, with the [10]CPP-PCL having a significantly ($p < 0.05$) higher fiber diameter than the [8]CPP-PCL,

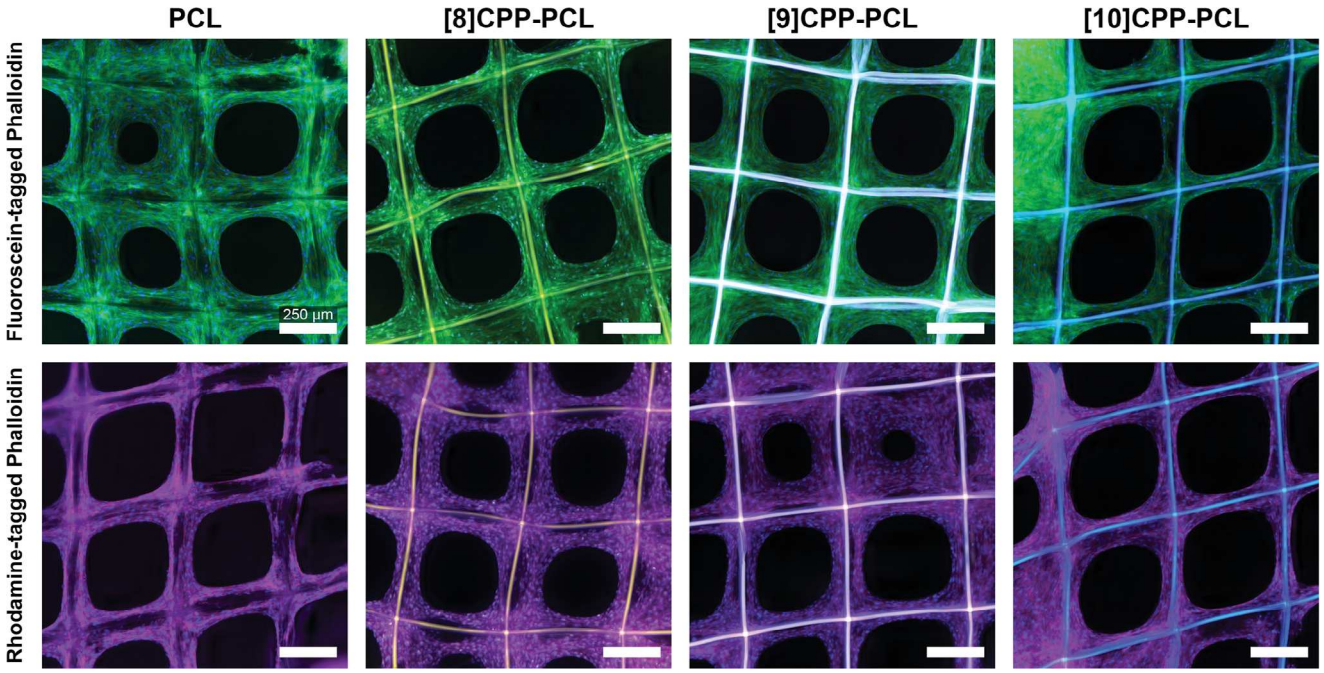

Figure 6. Fluorescent images of rhodamine- and fluorescein-tagged phalloidin stains conducted on PCL and [n]CPP-PCL scaffolds seeded with MSCs.

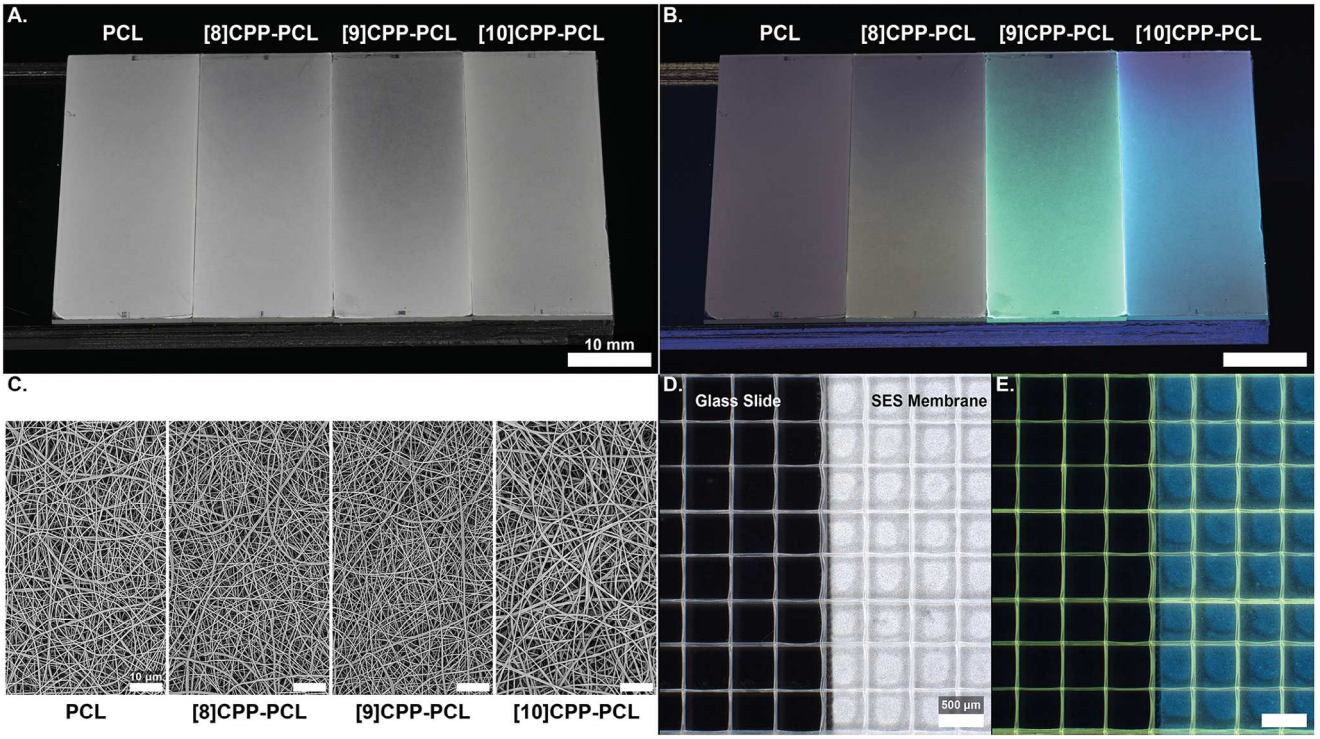

Figure 7. Solution electrospinning of [n]CPP-PCL. A,B) Control and [n]CPP-PCL membranes under visible and ultraviolet radiation. C) Representative SEM images of control and [n]CPP-PCL electrospun fibers. D) Ambient light image of [8]CPP-PCL MEW scaffold on [10]CPP-PCL solution electrospun substrate. E) Ultraviolet radiation image of [8]CPP-PCL MEW scaffold on [10]CPP-PCL solution electrospun substrate.

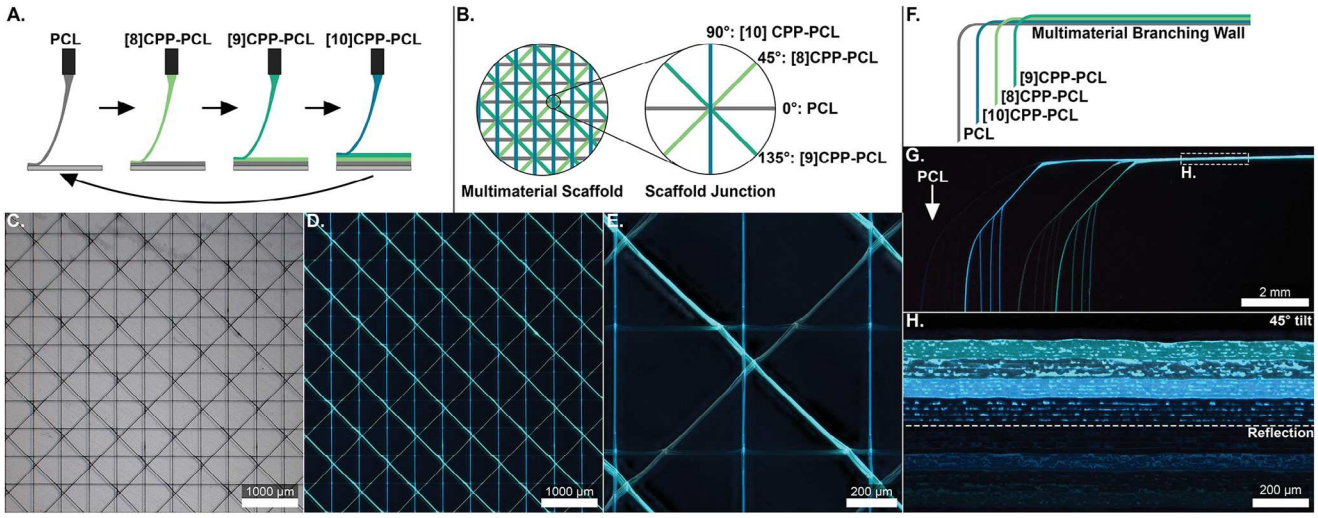

Figure 8. A) Sequential MEW of CPP-PCL materials using a multi-nozzle system. B) Schematic of multi-material MEW scaffold, with labeled fiber directions and materials. C) Brightfield image of multi-material MEW scaffold. D) Fluorescent image of multi-material MEW scaffold. E) Fluorescent image of multi-material MEW junction. F) Schematic of multi-material branching MEW wall. G) Fluorescent image of multi-material branching MEW wall. H) Tilted fluorescent image of multi-material MEW wall, with 4 distinct regions of fluorescence and non-fluorescence.

[9]CPP-PCL, and control PCL (Figure S6, Supporting Information). For the [10]CPP-PCL samples, this statistical difference is due to a bimodal distribution of fiber diameters (i.e., both smaller and large fiber diameters), while the average diameter was similar to [8]CPP-PCL and [9]CPP-PCL solutions, which is provided in Supporting Information File 2. This result could be attributed to either the [10]CPP within the material or, potentially, to the inherent variability that can occur for the SES process.[47] In general, the 300–400 nm fiber diameter achieved for SES and the good consistency of fiber diameter (Figure 7C) upon the addition of [n]CPP molecules demonstrates the utility of the fluorophores with this process, which is further shown in Figure S5 (Supporting Information). Furthermore, PCL is a widely used and important polymer for SES,[48] and the addition of the [n]CPPs did not substantially affect the capacity to produce high quality membranes.

As previously observed, performing MEW onto SES membrane substrates does not affect the quality of the scaffold,[25,45] and in this case we can assign different colors to the different components. When MEW was performed onto [10]CPP-PCL SES membranes using a [8]CPP-PCL blend, as expected the fibers and membrane could be readily contrasted with each other using the same incidence wavelength, exemplified in Figure 7D,E. The MEW fibers are directly visible against the SES membrane with specific fluorescent signals.

2.6. Establishing Multi-Material MEW Using [n]CPP-PCL Blends

The differently colored fluorophores aid in performing fundamental multi-material MEW research, generating proof-of-concept designs. By printing with all four materials, a composite scaffold with all three CPP colors and a control PCL can be achieved. **Figure 8** shows how four different MEW jets have been printed in a sequential and cyclic manner (Figure 8A), achieving semi-woven fiber intersections across a scaffold. This demonstrates multi-material MEW fiber printing control beyond a series of walls printed sequentially, but not interlocked.[49] While in this instance, all the fibers are made from PCL, the [n]CPP allows testing of multi-nozzle MEW concepts and generate G-code libraries while the technical issues surrounding processing different polymers, with differing melting points and thermal degradation profiles, are developed in parallel.

Another benefit of using [n]CPPs beyond their thermal stability is colorimetric orientation and waymarking for MEW scaffolds. When viewing samples under a microscope at higher magnifications, losing orientation with respect to the sample axis and boundaries is common, especially when the sample is embedded within tissue. Figure 8B–E shows a scaffold designed with lines at 4 angles: 0°, 45°, 90°, and 135°, with the color varying by angle. This capability helps investigate cell-scaffold interactions within a single scaffold. For example, fibers of different diameters or even polymer composition could be fluorescently tagged, which otherwise would be hard to distinguish under fluorescent imaging setting.

Another example is to validate the correct multi-material MEW printing strategies rather than establish this with expensive polymers. Figure 8F–H demonstrates how four differently colored fiber walls printed upon each other, branching out into separate fibers. Within this fiber wall, discrete fluorescent and non-fluorescent regions are shown in Figure 8G, that match our intended program. In addition to visualizing fiber-cell interactions, fluorescent MEW fibers and SES membranes can be used for fundamental processing and design research. There has been a spate of recent publications on using additives for MEW[28,50] and establishing and validating multi-material processing is aided by the validation of manufacture with fluorescent fibers. Since PCL is widely used for several processing approaches in biofabrication, the fluorescent properties of [n]CPPs are likely to be used in other forms beyond what is presented here.

3. Conclusion

This work outlines the application of a new class of fluorescent probes for MEW scaffolds that is compatible with the heating requirements of MEW, as demonstrated with a commonly investigated polymer, PCL. The fluorescent visualization of materials and substrates is a crucial aspect of biomedicine and biotechnology, and the [n]CPPs were effective in providing customizable fluorescence properties for MEW fibers while not causing toxicity or leaching. Even with the requirement for sustained elevated temperatures for MEW, the [n]CPP fluorophores provide ideal and unique outcomes for this technology. Interestingly, these fluorescent polymer blends are readily visualized with a low-cost handheld UV flashlight. Combining [n]CPPs with PCL provides a simple yet potent method to orient, visualize and better understand the interactions between MEW scaffolds and biological components, including cells and matrix proteins, compatible with existing imaging systems. In conclusion, enhancing visibility of MEW fibers within biological systems supports multi-channel fluorescence imaging that aids in our ability to study the evolving dynamics of cell-scaffold systems for tissue engineering and regenerative medicine.

4. Experimental Section

Materials: Poly(ε-caprolactone) (PCL) pellets were purchased from Corbion (Purasorb PC12, Lot # 2007001461). Dichloromethane (DCM) (Fisher, ACS certified, stabilized) and Dimethylformamide (DMF) (Fisher, ACS certified, stabilized) were used as received without further drying. [8]CPP, [9]CPP, and [10]CPP were synthesized according to previously established procedures.[35,37] These sizes with different number of phenylene rings were chosen as they provide a choice of fluorescent across commonly used imaging wavelengths, from 466 to 533 nm emissions. Experiments using "as received" PCL are referred to as PCL_{pellet}.

Blending of PCL and [n]CPPs: PCL was added to a round bottom flask equipped with a stir bar. DCM was added to a ratio of 20% w/v PCL, and the mixture stirred for 30 min to ensure adequate dissolution. A stock solution of [n]CPP in DCM (1 mg mL^{-1}) was prepared and injected into the mixture at the desired concentration. The resulting mixture was stirred for 30 min before the stir bar was removed and the solvent was removed under vacuum for several hours. To maximize the adequate removal of solvent, [n]CPP embedded PCL samples were subjected to molten thin film (<0.5 mm) spreading and placed in a vacuum oven at 80 °C for 7 days before use. A PCL control also underwent solvent mixing, referred to as PCL_{sham}.

Solution Electrospinning: [n]CPP-PCL was dissolved at 15% weight in a 60/40 vol% ratio of DCM and DMF to create the electrospinning "ink". These solvents were chosen to improve the processability of this ink, by modulating the solvent evaporation from the electrospinning fiber. This ink was then added to a 5-milliliter syringe with a 27-gauge dispensing nozzle (BSTEAN, blunt, stainless steel) attached and placed into a syringe pump (World Precision Instruments, AL-300, United States) and set to deliver 0.5 mL h^{-1}. The nozzle was connected to a Heinzinger LNC 20000 – three negative high voltage power supply unit. For the electrospun mesh collection, a rotating 6-slide grounded collector was placed 14 cm away from the nozzle, and the slides were mounted by hydrostatic force between the metal collector and the glass slides. SES was performed for 30 min at 18 kV under these conditions. Sputter coating (Cressington, Watford, UK) of the SES membranes with Au-Pd was used to enable imaging by scanning electron microscopy (SEM) (ThermoFisher Apreo 2), while fiber diameter was determined from images using the Icy technique.[51] The fibers used for diameter measurements were chosen by drawing two perpendicular lines, crossing in the center of the image, and measuring the first ten fibers that intersect this cross, moving outward in a clockwise pattern.

Melt Electrowriting: The blended [n]CPPs and PCL formulations included a PCL control that also underwent solvent mixing, termed PCL_{sham}. As discussed above, polymers were loaded into 3 mL syringes (Nordson Continuum EFD) with a 25-gauge nozzle (Nordson EFD Precision Tip) and a pneumatic plunger. The loaded syringes were placed in an oven at 80 °C overnight prior to processing that was performed at 80 °C with 2 bars of pneumatic air pressure. A voltage of 6.0 kV was used across a gap of 4 mm to establish an electric field of 1.5 kV mm^{-1} between the charged head and grounded metal collector. The jet speed was determined at a first occurrence of the straight printed fiber when the printing speed was varied from 350 to 700 mm min^{-1}, with 10 mm min^{-1} steps. After determination of the jet speed for blending of PCL and [n]CPPs at 630 mm min^{-1}, a collector speed of 640 mm min^{-1} was used to generate all planar scaffolds and structures. Multi-material MEW was conducted on a custom multi-nozzle system, where all syringes with different fluorophores and a PCL control that also underwent solvent mixing (termed PCL_{sham}) were heated and pressurized simultaneously.

The fabrication of MEW tubes was performed on a custom-built system with a cylindrical collector. These processing parameters used the same polymer blend but adopted a 22-gauge nozzle in combination with a 3 mm distance from the nozzle to the metal mandrel. A metal cylinder with a diameter of 5 mm was used as the collector, while the toolpath for the scaffolds were designed with MATLAB. The tubular MEW processing parameters included a 4.5 kV voltage applied to the nozzle, an air pressure of 0.5 bar, and a heater temperature of 80 °C. Optical imaging of the fibers and scaffolds was performed on a Keyence VHX-7000, which was complemented with a 365 nm flashlight to image the fiber fluorescence.

Differential Scanning Calorimetry: To analyze the thermal properties of the materials, a TA Instruments Discovery 2500 differential scanning calorimeter was used. Samples of all materials were cut and weighed, then placed in hermetic pans and sealed. These samples were then loaded into the DSC system and set to run. The running conditions were in three steps, all conducted at a ramp of 10 °C min^{-1}: step one ranged from −80 to 150 °C, step two ranged from 150 to −80 °C, and step three ranged from −80 to 150 °C. This repeat was used to standardize the thermal treatment in analyzing the crystallinity and melting temperatures. The melting temperature analysis was conducted on step three's data. These tests were run in triplicate for each material, and characterized using TRIOS analysis software to find the melting temperatures and crystallinity. The data was plotted with GraphPad Prism.

Thermogravimetric Analysis: A TA Instruments Q500 thermogravimetric analyzer was used to investigate the thermal degradation of the materials. An aluminum pan was placed in a platinum tray and tared, then 5–10 mg of material was added to the pan. The system was set to ramp at 10 °C min^{-1} to 600 °C, with the ramp starting at room temperature. The mass loss was analyzed with Microsoft Excel, and plotted with GraphPad Prism.

Viscometric Analysis: The viscosity of the materials was characterized using a TA Instruments DHR-2 rheometer. The environmental thermal system was used to heat the plates into the range needed for the experiments, with 25 mm diameter parallel plates and a 500 µm gap. For analyzing the rheological responses to changing temperatures, a shear rate of 1 s^{-1} was used, while the temperature was changed at a ramp of 5 °C min^{-1}, and the viscosity was measured at an interval of 1 °C. To further analyze the viscosity within the chosen thermal conditions, a processing temperature of 80 °C was used, and the shear rate was varied from 0.001 to 10 s^{-1}. The data was statistically analyzed and plotted in GraphPad Prism.

Cytotoxicity: Cytotoxicity tests were designed in accordance with ISO 10993-5 and ISO 10993-12. Extract tests were conducted to eliminate variance from PCL surface hydrophobicity. Sheets of the [n]CPP-PCL and PCL control were first sterilized by soaking in 70% ethanol for 30 min, then washed three times with sterile 1x phosphate buffered saline (PBS). The samples were then submerged in serum-free media for 72 h at 37 °C with the surface area-to-volume ratio of 3 cm^2 mL^{-1} as described in ISO 10993-12. The eluant media was composed of Dulbecco's Modified Eagle Media (DMEM) with 1% penicillin-streptomycin. The extraction media was collected and supplemented with 10% v/v fetal bovine serum before application to cells. The cells (Adipose Derived Adult Stem Cells: Zen Bio,

Lot#ASC062118A) were seeded at 4000 cells per well in a 96 well plate and cultured to 80% confluency and exposed to the extraction media. Primary controls included the addition of 1% or 15% v/v phosphate buffered saline, and 1%, 5%, and 10% v/v ethanol for positive cell inhibition. Nitrile rubber (Kimtech Purple Nitrile Exam Gloves) and poly(vinyl chloride) (Home Depot PVC, USA) were used as secondary elution controls. After 48 h of eluant media exposure to cells, AlamarBlue was used as an indicator of cellular inhibition and cytotoxicity, based on previously established methods.[52,53] DMEM base medium (with 1% PS and 10% FBS), without ethanol, PCL or [n]CPP-PCL elutes, was used as baseline to calculate % growth inhibition according to:

$$\textit{Relative Metabolic Activity}\ \ (\%) = \ 100\,x\left(\frac{A_{sample}}{A_{base}}\right) \tag{1}$$

where A_{sample} is the metabolic activity measured for each sample and control sample well and A_{base} is the metabolic activity measured for cells cultured in normal DMEM base medium (with 1% PS and 10% FBS). Inhibition of MSCs was then presented as a function of PCL or [n]CPP-PCL elutes added to living cells in relation to the baseline (A_{base}).

Cell-Scaffold Visualization When Using CPP-PCL: Further cell testing utilized fluorescent MEW scaffolds composed of a crosshatch design with 500 microns spacing and five layers. These were punched to 5 mm diameter and sterilized with 70% ethanol for 30 min. Surface treatment with 0.1 M sodium hydroxide was utilized to improve cell attachment by reducing the hydrophobicity of PCL scaffolds. NaOH treated scaffolds were washed in PBS overnight, prior to downstream applications with cells. MSC's were seeded at a density of 60 000 cells/scaffold in DMEM base medium. These scaffolds were seeded with a droplet method, where a 12 µL droplet of cell suspension was pipetted onto the dry scaffold. Every 2nd hour for 6 h, the seeded scaffolds were given a 5 µL droplet of media to prevent drying out. At 6 h, once the cells have had time to attach to the scaffolds, excess media was added and the samples were allowed to culture. After 1 day, the media was changed to include fibroblast growth factor beta (1 ng mL^{-1}) and scaffolds were cultured for up to 7 days. Scaffolds approaching confluency were fixed in 10% formalin for 30 min, then stored in PBS with 0.03 M glycine. To analyze the development of the cellular structures, phalloidin and 4′,6-diamidino-2-phenylindole (DAPI, Biolegend, USA) staining was chosen. Two variants of phalloidin were used, with fluorescein (Biotium CF488, USA, lot # 21P0309-1145133) and rhodamine (Biotium CF594, USA, lot # 20R0928-1145053) fluorescent tags to evaluate the usability of [n]CPP-PCL in relation to common fluorophores. Samples were permeabilized in 0.1% Triton X (VWR, USA) for 10 s, washed in 2 wt% Bovine Serum Albumin (BSA, VWR, USA) blocking buffer for 30 min at room temperature and incubated with fluorescent probes (DAPI: 1 µg mL^{-1}, fluorescein-phalloidin: 5 µg mL^{-1}, and rhodamine-phalloidin: 5 µg mL^{-1}) for 10–20 min. Imaging used an EVOS XL Core for brightfield images and a Leica Thunder Imager for fluorescent imaging. For fluorescent imaging, DAPI, fluorescein, and rhodamine were imaged on prebuilt channels for these fluorophores. To image the [n]CPP-PCL materials, an excitation wavelength of 395 nm was used, with fluorescent filters for 535 nm (FITC), 590 nm (TRITC), and 642 nm (CY5) to image [10]CPP-PCL, [9]CPP-PCL, and [8]CPP-PCL respectively.

Fluorophore Leaching: Leaching tests were conducted utilizing the 3 cm^2 mL^{-1} surface area-to-volume ratio approach established in ISO10993-12. Sheets of polymer were cut into 3 cm^2 pieces, placed in a 1.5 mL tube, then immersed in 1 mL of PBS for 7 days at 37 °C. Next, the pieces were removed, and the PBS transmission was measured with a UV spectrometer (Agilent Cary 60 UV–vis Spectrophotometer).

Statistical Analysis: Analysis of the statistical significance of all quantified data used GraphPad Prism. For analyzing difference between multiple groups, analysis of the distribution and normality were followed by the respective analysis of variance (ANOVA) test. For Figure 5, the statistical analysis was a Kruskal Wallis one way ANOVA. For Figures S1 and S5 (Supporting Information), fiber diameters were analyzed by an ordinary one-way ANOVAs. Multiple comparisons were done through Tukey's post-hoc testing for all samples. Significance was denoted as follows: $^{*} = p < 0.05$, $^{**} = p < 0.01$, $^{***} = p < 0.001$, $^{****} = p < 0.0001$. The term "n" was used to refer to sample size.

Supporting Information

Supporting Information is available from the Wiley Online Library or from the author.

Acknowledgements

The technical assistance of Simon Luposchainsky and the insights of Michael Haley were invaluable. Thank you to Casey Check and the Center for Advanced Materials Characterization in Oregon for their support on this work. The financial support from the Wu Tsai Human Performance Alliance and the Joe and Clara Tsai Foundation is greatly appreciated. P.D. was supported by the Bradshaw and Holzapfel Research Professor in Transformational Science and Mathematics Fund. H.W.R. and R.J. were supported by the U.S. National Science Foundation (CHE-2102567).

Conflict of Interest

The authors declare no conflict of interest.

Data Availability Statement

The data that support the findings of this study are available from the corresponding author upon reasonable request.

Keywords

additive manufacturing, biofabrication, electrospinning, scaffolds, tissue engineering

Received: February 2, 2024
Revised: April 27, 2024
Published online:

[1] D. H. Reneker, I. Chun, *Nanotechnology* **1996**, *7*, 216.
[2] J. Xue, T. Wu, Y. Dai, Y. Xia, *Chem Rev* **2019**, *119*, 5298.
[3] Y. Q. Wu, R. L. Clark, *J. Biomater. Sci.-Polym. Ed.* **2008**, *19*, 573.
[4] L. Larrondo, R. S. J. Manley, *J. Polym. Sci. Part B-Polym. Phys.* **1981**, *19*, 909.
[5] T. D. Brown, P. D. Dalton, D. W. Hutmacher, *Adv. Mater.* **2011**, *23*, 5651.
[6] S. Lee, *J. Appl. Polym. Sci.* **2009**, *114*, 3652.
[7] S. Lee, S. K. Obendorf, *J. Appl. Polym. Sci.* **2006**, *102*, 3430.
[8] X. H. Li, W. M. Yang, H. Y. Li, Y. Wang, M. M. Bubakir, Y. M. Ding, Y. C. Zhang, *J. Appl. Polym. Sci.* **2015**, *132*, 41601.
[9] M. L. Jorgensen, C. Muller, M. Sikkersoq, M. Nadzieja, Z. Zhang, Y. Su, J. Just, K. L. Garm Spindler, M. Chen, *Mater Today Bio* **2020**, *6*, 100052.
[10] A. Tamayol, M. Akbari, N. Annabi, A. Paul, A. Khademhosseini, D. Juncker, *Biotechnol. Adv.* **2013**, *31*, 669.
[11] F. Girard, C. Lajoye, M. Camman, N. Tissot, F. B. Pedurand, B. Tandon, D. Moedder, I. Liashenko, S. Salameh, P. D. Dalton, M. Rielland, *Adv. Funct. Mater.* **2024**, 2314757.
[12] N. Bhardwaj, S. C. Kundu, *Biotechnol. Adv.* **2010**, *28*, 325.
[13] J. A. Matthews, G. E. Wnek, D. G. Simpson, G. L. Bowlin, *Biomacromolecules* **2002**, *3*, 232.

[14] D. H. Reneker, A. L. Yarin, *Polymer* **2008**, *49*, 2387.
[15] S. V. Fridrikh, J. H. Yu, M. P. Brenner, G. C. Rutledge, *Phys. Rev. Lett.* **2003**, *90*, 144502.
[16] P. D. Dalton, *Curr. Opin. Biomed. Eng.* **2017**, *2*, 49.
[17] Á. G. Marín, D. Lohse, *Phys. Fluids* **2010**, *22*, 122104.
[18] G. Taylor, *Proc. Royal Soc.London* **1969**, *313*, 453.
[19] T. Tylek, C. Blum, A. Hrynevich, K. Schlegelmilch, T. Schilling, P. D. Dalton, J. Groll, *Biofabrication* **2020**, *12*, 025007.
[20] H. Lu, Y. Sun, Y. Chen, L. Nie, L. Yang, L. Du, H. Xu, *Mater. Lett.* **2023**, *334*, 133738.
[21] A. Youssef, A. Hrynevich, L. Fladeland, A. Balles, J. Groll, P. D. Dalton, S. Zabler, *Tissue Eng., Part C* **2019**, *25*, 367.
[22] L. A. Bosworth, S. Downes, *Polymer Degradation and Stability* **2010**, *95*, 2269.
[23] N. Golafshan, M. Castilho, A. Daghrery, M. Alehosseini, T. van de Kemp, K. Krikonis, M. de Ruijter, R. Dal-Fabbro, A. Dolatshahi-Pirouz, S. B. Bhaduri, M. C. Bottino, J. Malda, *ACS Appl. Mater. Interfaces* **2023**, *15*, 12735.
[24] D. Loessner, A. Rockstroh, A. Shokoohmand, B. M. Holzapfel, F. Wagner, J. Baldwin, M. Boxberg, B. Schmalfeldt, E. Lengyel, J. A. Clements, D. W. Hutmacher, *Biomaterials* **2019**, *190–191*, 63.
[25] I. Pennings, E. E. van Haaften, T. Jungst, J. A. Bulsink, A. J. W. P. Rosenberg, J. Groll, C. V. C. Bouten, N. A. Kurniawan, A. I. P. M. Smits, D. Gawlitta, *Biofabrication* **2019**, *12*, 015009.
[26] N. T. Saidy, A. Fernández-Colino, B. S. Heidari, R. Kent, M. Vernon, O. Bas, S. Mulderrig, A. Lubig, J. C. Rodríguez-Cabello, B. Doyle, D. W. Hutmacher, E. M. de-Juan-Pardo, P. Mela, *Adv. Funct. Mater.* **2022**, *32*, 2110716.
[27] D. Olvera, M. S. Molina, G. Hendy, M. G. Monaghan, *Adv. Functional Mater.* **2020**, *30*, 1909880.
[28] M. Zhu, Z. Hu, N. Liu, K. Yao, G. Hong, Y. Li, Y. Chen, H. He, W. Wu, Y. Zhou, J. Shi, Y. He, *Small* **2024**, e2400644.
[29] E. Dondossola, S. Alexander, B. M. Holzapfel, S. Filippini, M. W. Starbuck, R. M. Hoffman, N. Navone, E. M. De-Juan-Pardo, C. J. Logothetis, D. W. Hutmacher, P. Friedl, *Sci. Transl. Med.* **2018**, *10*.
[30] D. Janzen, E. Bakirci, A. Wieland, C. Martin, P. D. Dalton, C. Villmann, *Adv. Healthcare Mater.* **2020**, *9*, e1901630.
[31] C. Vaquette, W. Fan, Y. Xiao, S. Hamlet, D. W. Hutmacher, S. Ivanovski, *Biomaterials* **2012**, *33*, 5560.
[32] X. Wu, T. Vedelaar, R. Li, R. Schirhagl, M. Kamperman, M. K. Włodarczyk-Biegun, *Bioprinting* **2023**, *32*, e00288.
[33] D. Nahm, F. Weigl, N. Schafer, A. Sancho, A. Frank, J. Groll, C. Villmann, H. W. Schmidt, P. D. Dalton, R. Luxenhofer, *Materials Horizons* **2020**, *7*, 928.
[34] B. M. White, Y. Zhao, T. E. Kawashima, B. P. Branchaud, M. D. Pluth, R. Jasti, *ACS Central Sci.* **2018**, *4*, 1173.
[35] J. Xia, J. W. Bacon, R. Jasti, *Chem. Sci.* **2012**, *3*, 3018.
[36] J. Mun, J. Kang, Y. Zheng, S. Luo, H.-C. Wu, N. Matsuhisa, J. Xu, G.-J. N. Wang, Y. Yun, G. Xue, J. B.-H. Tok, Z. Bao, *Adv. Mater.* **2019**, *31*, 1903912.
[37] E. R. Darzi, T. J. Sisto, R. Jasti, *J. Org. Chem.* **2012**, *77*, 6624.
[38] T. Iwamoto, Y. Watanabe, Y. Sakamoto, T. Suzuki, S. Yamago, *J. Am. Chem. Soc.* **2011**, *133*, 8354.
[39] L. Adamska, I. Nayyar, H. Chen, A. K. Swan, N. Oldani, S. Fernandez-Alberti, M. R. Golder, R. Jasti, S. K. Doorn, S. Tretiak, *Nano Lett.* **2014**, *14*, 6539.
[40] H. Rupp, W. H. Binder, *Adv. Mater. Technol.* **2020**, *5*, 2000509.
[41] N. C. Paxton, J. Ren, M. J. Ainsworth, A. K. Solanki, J. R. Jones, M. C. Allenby, M. M. Stevens, M. A. Woodruff, *Macromol. Rapid Commun.* **2019**, *40*, e1900019.
[42] C. Bohm, P. Stahlhut, J. Weichhold, A. Hrynevich, J. Tessmar, P. D. Dalton, *Small* **2022**, *18*, e2104193.
[43] C. Böhm, B. Tandon, A. Hrynevich, J. Teßmar, P. D. Dalton, *Macromolecular Chem. Phys.* **2022**, *223*, 2100417.
[44] T. C. Lovell, S. G. Bolton, J. P. Kenison, J. Shangguan, C. E. Otteson, F. Civitci, X. Nan, M. D. Pluth, R. Jasti, *ACS Nano* **2021**, *15*, 15285.
[45] T. Jungst, I. Pennings, M. Schmitz, A. J. W. P. Rosenberg, J. Groll, D. Gawlitta, *Adv. Funct. Mater.* **2019**, *29*, 1905987.
[46] L. Yang, Y. Lou, G. Zhang, Y. Sun, Y. Yang, J. Wu, Y. Ye, X. Chu, L. Du, Z. Jiang, H. Xu, *Colloids Surf. A* **2024**, *680*, 132655.
[47] S. De Vrieze, T. Van Camp, A. Nelvig, B. Hagström, P. Westbroek, K. De Clerck, *J. Mater. Sci.* **2009**, *44*, 1357.
[48] M. J. Moore, Y. T. Lam, M. Santos, R. P. Tan, N. Yang, J. Hung, Z. Li, K. A. Kilian, J. Rnjak-Kovacina, J. B. Pitts, H. Menzel, S. G. Wise, *ACS Biomater. Sci. Eng.* **2023**, *9*, 3320.
[49] P. G. Saiz, A. Reizabal, S. Luposchainsky, J. L. Vilas-Vilela, S. Lanceros-Mendez, P. D. Dalton, *Adva. Mater. Technol.* **2023**, *8*, 2202063.
[50] G. Cedillo-Servin, O. Dahri, J. Meneses, J. van Duijn, H. Moon, F. Sage, J. Silva, A. Pereira, F. D. Magalhães, J. Malda, N. Geijsen, A. M. Pinto, M. Castilho, *Small* **2024**, *20*, 2307178.
[51] F. de Chaumont, S. Dallongeville, N. Chenouard, N. Hervé, S. Pop, T. Provoost, V. Meas-Yedid, P. Pankajakshan, T. Lecomte, Y. Le Montagner, T. Lagache, A. Dufour, J.-C. Olivo-Marin, *Nat. Methods* **2012**, *9*, 690.
[52] F. Bonnier, M. E. Keating, T. P. Wróbel, K. Majzner, M. Baranska, A. Garcia-Munoz, A. Blanco, H. J. Byrne, *Toxicol. In Vitro* **2015**, *29*, 124.
[53] S. N. Rampersad, *Sensors* **2012**, *12*, 12347.